Articles

Molecular-Level Organization of Saturated and Polyunsaturated Fatty Acids in a Phosphatidylcholine Bilayer Containing Cholesterol†

Michael C. Pitman and Frank Suits

IBM T. J. Watson Research Center, Yorktown Heights, New York 10598

Alexander D. MacKerell, Jr.

Department of Pharmaceutical Sciences, School of Pharmacy, University of Maryland, Baltimore, Maryland 21201

Scott E. Feller*

Department of Chemistry, Wabash College, Crawfordsville, Indiana 47933

Received August 16, 2004; Revised Manuscript Received September 27, 2004

ABSTRACT: Cholesterol's preference for specific fatty acid chains is investigated at the atomic level in a 20 ns molecular dynamics computer simulation of a lipid bilayer membrane consisting of cholesterol and 1-stearoyl-2-docosahexaenoyl-*sn*-glycero-3-phosphocholine (SDPC) in a 1:3 ratio. These simulations reproduce experimental measurements suggesting that cholesterol prefers to be solvated by saturated acyl chains and has a low affinity for polyunsaturated fatty acids. Analyses of the simulation trajectory provide a detailed picture of both the transverse and lateral structures of the lipid bilayer membrane, along with a description of lipid and cholesterol dynamics at high temporal resolution. Comparison with a previous simulation of a pure phospholipid bilayer allows an atomic-level description of the changes in membrane structure and dynamics resulting from incorporation of cholesterol. The observed differential cholesterol interactions with saturated and polyunsaturated lipids provide a mechanism for the formation of laterally inhomogeneous membranes; thus, the simulation provides molecular-level insight into the formation of lipid rafts.

Cholesterol has long been acknowledged to play a key role in determining eukaryotic membrane structure and dynamics, allowing regulation of integral membrane protein activity through composition, in the essentially isothermal/isobaric environment of the cell. Recently, the level of interest in cholesterol has increased further because of its ability to trigger domain formation in lipid bilayer membranes (*1*). The inhomogeneous lateral distribution of lipid components, e.g., raft formation, typically into regions characterized by differing levels of molecular order, has been proposed to be important in the function of membrane proteins (*2*). While the formation of this complex structure is undoubtedly a complicated function of forces among lipids, proteins, and cholesterol, a large class of experimental measurements suggests that specific interactions between cholesterol and polyunsaturated phospholipid acyl chains may be one critical component in domain formation (*3*−*5*).

Polyunsaturated fatty acids (PUFA)[1] are known to play an integral role in a wide variety of biological functions. The most studied PUFA is docosohexaenoic acid (DHA), an ω-3 chain 22 carbons in length with six double bonds. Insufficient levels of DHA are associated primarily with decreased brain development (*6*) and visual acuity (*7*); however, the dietary DHA level has been associated with pathologies ranging from rheumatoid arthritis (*8*) to cystic fibrosis (*9*). That a single molecule could be involved in such a diverse array of biological processes suggests it acts at a very fundamental level, such as by determining physical properties of cell membranes (for an excellent review of DHA and its effects, see ref *10*). One possibility is that DHA promotes lateral segregation in biological membranes due to unfavorable interactions with cholesterol. Previous experimental and simulation studies have shown that the DHA chain is extremely flexible, characterized by a high degree of molecular disorder and a rapid interconversion among a

† This work was supported by the National Science Foundation and the National Institutes of Health through Grant MCB-0091508 to S.E.F. and Grant GM515001 to A.D.M., respectively.

* To whom correspondence should be addressed: Department of Chemistry, Wabash College, 301 W. Wabash Ave., Crawfordsville, IN 47933. Phone: (765) 361-6175. Fax: (765) 361-6149. E-mail: fellers@wabash.edu.

[1] Abbreviations: MD, molecular dynamics; NMR, nuclear magnetic resonance; PUFA, polyunsaturated fatty acids; DHA, docosohexaenoic acid; CHARMM, Chemistry at Harvard Molecular Mechanics; SDPC, 1-stearoyl-2-docosahexaenoyl-*sn*-glycero-3-phosphocholine; PD, probability density; NOESY, nuclear Overhauser enhancement spectroscopy; PC, phosphatidylcholine.

10.1021/bi048231w CCC: $27.50
Published on Web 11/12/2004

diverse set of conformational states (*11*). These results suggest a fundamental incompatibility between the highly disordered DHA acyl chains and the rigid planar shape of the cholesterol molecule.

In the following we describe a molecular dynamics (MD) computer simulation that provides insight into the atomic-level organization of a hydrated lipid bilayer membrane containing a mixed chain (saturated and polyunsaturated) phosphatidylcholine and cholesterol in a 3:1 ratio. This study, addressing the interactions between DHA and cholesterol, follows from previous simulation studies of DHA in a phosphatidylcholine bilayer (*11*) and of DHA−protein interactions (*12*). We chose the composition of the model membrane both to study a lipid of significant biological relevance (polyunsaturated fatty acids are found most commonly at the *sn*-2 position of the phospholipid typically paired with a saturated fatty acid) and to avoid the prohibitively long equilibration times that would be required in studying a mixture of disaturated and di-polyunsaturated lipids. This study was made possible by our development of empirical force field parameters for the cholesterol molecule, consistent with the CHARMM27 parameter set for lipids (*11*, *13*−*15*), that are provided here as Supporting Information. In addition to demonstrating excellent agreement between the simulation and various observables from NMR spectroscopy, we describe several important simulation results that highlight the unique nature of the interaction between cholesterol and polyunsaturates. We conclude with a discussion of the relevance of these observations to domain formation in cell membranes.

EXPERIMENTAL PROCEDURES

System construction was carried out using CHARMM (*16*, *17*) based on initial lipid and water conformations taken from an earlier simulation (*11*) and the energy-minimized cholesterol conformation provided in the Supporting Information. The CHARMM27 lipid force field was employed for all simulations (*11*, *13*−*15*) supplemented with the cholesterol parameters developed as part of this work (see below). The system consisted of 72 1-stearoyl-2-docosahexaenoyl-*sn*-glycero-3-phosphocholine (SDPC) lipid molecules, 24 cholesterol molecules, and 2174 water molecules (30.2 H_2O molecules/lipid, corresponding to a fully hydrated bilayer). The initial dimensions of the simulation cell were determined by assuming surface areas per molecule of 67.2 and 32.0 $Å^2$/molecule for SDPC and cholesterol, respectively, based on experimental data and previous simulation results (*11*, *18*, *19*). The cholesterol molecules were placed on a hexagonal lattice with the addition of random offsets from the lattice on the order of 3 Å, after scaling the locations of the centers of mass of the lipids and water in the $x-y$ plane (parallel to the bilayer). Energy minimization followed to remove bad contacts. A 2 ns constant normal pressure (1 atm) simulation was carried out with CHARMM to allow the system density to equilibrate. The length of the unit cell quickly (<200 ps) came to equilibrium and fluctuated around its average value of 63.76 ± 0.01 Å. Analysis of the surface tension (20 ± 2 dyn/cm) and the deuterium order parameters (described in a subsequent section), both quantities which have been shown to be sensitive to the surface area (*20*), suggested that reasonable lateral dimensions had been chosen for the unit cell. Further equilibration at a constant volume was then carried out during a 2 ns MD simulation at a constant temperature (310 K) with the Blue Matter package (*21*), via velocity resampling at 1 ps intervals. A 20 ns production run was conducted in the NVE ensemble with Blue Matter, using a 52.96 Å × 52.96 Å × 62.7028 Å simulation cell. During the initial 7.5 ns of this simulation, there was additional reorganization of the membrane components, including a temporary exchange of a cholesterol molecule from one monolayer to another, as molecules relaxed from the initial model-built configuration. After equilibration for 11.5 ns, the system was stable and a final 12.5 ns was obtained for the analysis presented here. We have previously shown (*22*) that trajectories 10 ns in length are sufficient for obtaining the dipolar correlation functions needed to calculate the NMR cross-relaxation rates that are of primary interest in this work; thus, the simulation was ended after 12.5 ns of equilibrium trajectory. The use of the NVE ensemble, while somewhat novel for membrane simulations, ensures that dynamical properties, such as the time correlation functions that are needed to calculate several NMR observables, are not perturbed by the extended system algorithms used to produce constant-temperature and/or -pressure ensembles (*23*).

Optimization of the empirical force field parameters was performed using CHARMM. Geometry optimizations were performed in the gas phase using the Newton−Raphson minimizer to a rms gradient of 10^{-6} kcal mol^{-1} $Å^{-1}$ with no truncation of nonbond interactions. Assignments of the vibrational spectra were determined using the MOLVIB module (*24*) using the definitions of Pulay et al. (*25*). Quantum mechanical calculations were performed with the Gaussian 98 package (*26*) with geometry optimizations performed to default tolerances. Target bond lengths and valence angles for the steroid moiety of cholesterol were obtained from a survey of the Cambridge Structural Database (CSD) (*27*). The survey selected all structures that have the connectivity of the carbon atoms in the steroid moiety, including the C5−C6 double bond, with the hydroxyl and methyl groups omitted and with an *R*-factor of <7.5%.

RESULTS

Empirical Force Field Parameters for Cholesterol. Prior to the MD simulations, the CHARMM27 force field for lipids was extended to include cholesterol. Available parameters from the alkanes and alkenes were applied directly to cholesterol. This included the assignment of charges based on previously published approaches (*15*, *28*, *29*) and, initially, creation of the required parameters for cholesterol based on analogy with available parameters. Alcohol charges were transferred directly from threonine. Optimization of the new internal parameters was then performed to reproduce geometric data for bonds and angles involving carbons in the steroid skeleton from a survey of the CSD and scaled quantum mechanical (QM) spectra from the HF/6-31G* level of theory on a compound that excluded the cholesterol side chain (i.e., C20 and beyond; see residue CHNS in Table 3 of the Supporting Information). Presented in Table 1 of the Supporting Information are the CSD and CHARMM geometries for the bonds and valence angles involving carbon atoms in the steroid moiety. For the bond lengths, the CHARMM values agree with the CSD data within the standard deviations of the survey results. Similar agreement

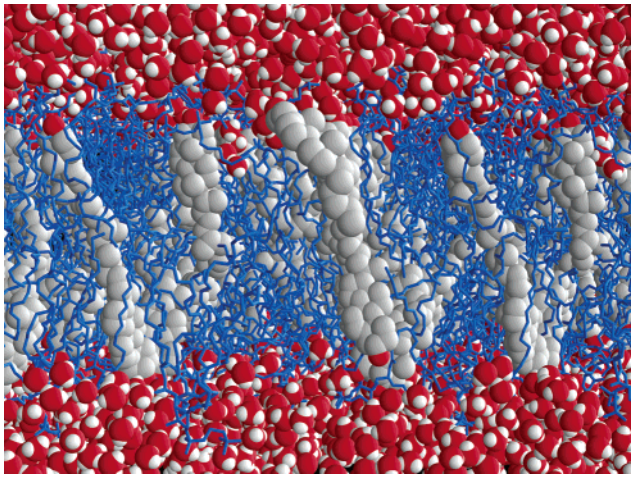

FIGURE 1: Snapshot of the system at the 12.5 ns point.

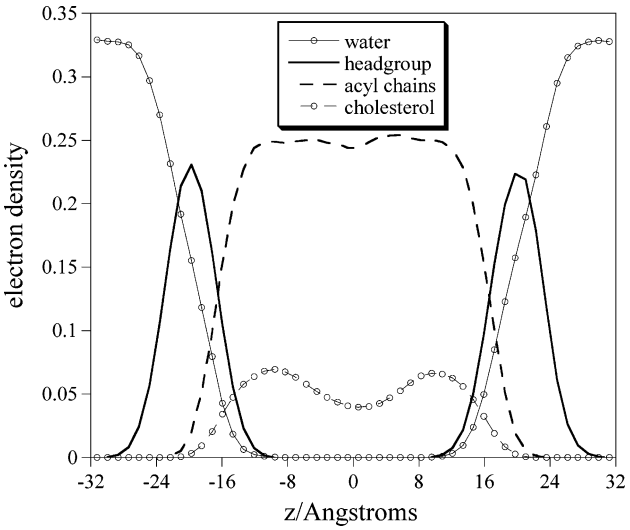

FIGURE 2: Distribution of molecular groups along the *z*-coordinate (bilayer normal). The water, lipid headgroup, lipid acyl chains, and cholesterol are denoted by a solid line with circles, a solid line, a dashed line, and a dashed line with circles, respectively.

occurs with the valence angles, with the exception of three terms. A comparison of the QM and empirical vibrational spectra is presented in Table 2 of the Supporting Information. The comparison includes the assignments of the individual modes. For the low-frequency region of the spectra, the agreement between the QM and empirical data is quite good, with the empirical vibrations being slightly higher than the QM values. The quality of agreement of the low-frequency regions is important as these correspond to the larger magnitude motions that occur in the molecule during MD simulations. Further improvements in the level of agreement between the QM and empirical data were not possible due to maintenance of the previously optimized internal parameters such that only the novel parameters (see Table 4 of the Supporting Information) were adjusted in this work. Overall, the parameters for cholesterol adequately reproduce both the geometric and vibrational target data, indicating the model will perform satisfactorily in MD simulations. Importantly, the application of nonbond parameters consistent with the remainder of the CHARMM27 lipid parameters ensures that interactions of cholesterol with the surrounding environment will be properly treated. The parameters were then tested via MD simulation (described below) in which excellent results were obtained with the exception of the distribution of torsion angles for the hydroxyl group. The torsional parameters were then adjusted on the basis of QM calculations on the model compound (see Figure 1 of the Supporting Information). The final parameter set is provided in the Supporting Information and is available at http://www.pharmacy.umaryland.edu/faculty/amackere/research.html.

Molecular Dynamics Simulation Results. Figure 1 gives a snapshot of the system at the 12.5 ns point of the NVE run, showing a stable bilayer membrane in the fluid state. Monitoring of the energy and temperature during the NVE production phase of the simulation showed only small fluctuations ($\sigma = 2.73$ kcal/mol and 1.63 K for energy and temperature, respectively) and negligible drift, indicating a well-equilibrated system and a robust integration scheme. Turning from these technical details of the simulation procedure, we describe in the following paragraphs the transverse structure of the membrane, i.e., the locations along the bilayer normal where the cholesterol resides. We then see how these observations affect the deuterium order parameters and NOESY cross-relaxation rates and compare the simulated quantities with experiment. Probability density isosurfaces are then used to describe the lateral organization of the membrane with atomic detail. We conclude with observations of the dynamical properties of the cholesterol and phospholipids.

Figure 2 shows the time-averaged density distribution as a function of the *z* coordinate (bilayer normal) for water, cholesterol, and lipid headgroup and acyl chains. The cholesterol is located primarily in the upper acyl chain region, balancing the tendency for the ring system to occupy the hydrophobic core with the hydroxyl group's need to hydrogen bond to water and/or the polar lipid groups. The cholesterol OH group is found approximately coincident with the lipid carbonyl groups (16.2 and 16.0 Å, respectively) in the interfacial region of significant heterogeneity. The cholesterol hydroxyl group is quite mobile, interacting strongly with water approximately 50% of the time, with the remainder split nearly evenly between lipid phosphate and carbonyl groups. These observations are in general consistent with previous simulation studies, carried out with the disaturated lipid dipalmitoylphosphatidylcholine (DPPC). One notable difference is the lack of chain specificity for hydrogen bonding with the carbonyl groups observed in the simulation presented here, as opposed to early work of Tu et al. (*18*) and recent simulations of Berkowitz and co-workers (*30*) which showed a strong preference for interaction with the *sn*-1 and *sn*-2 carbonyl, respectively (details of the chain structure, explored in the following paragraphs, provide an explanation of these differences between disaturated and mixed chain systems). Wassall and co-workers have probed the insertion of cholesterol into a related mixed chain system, stearoylarachadonylphosphatidylcholine (SAPC), using neutron scattering techniques (personal communication). They find that the center of mass of deuterons at the 2, 2, 3, 4, 4, and 6 positions on the sterol lies 2 Å below the phospholipid carboxyls, in good agreement with the distance of 1.5 Å observed in our simulation of the somewhat more unsaturated system (six vs four double bonds). Our observation of the cholesterol hydroxyl group inserting to the level

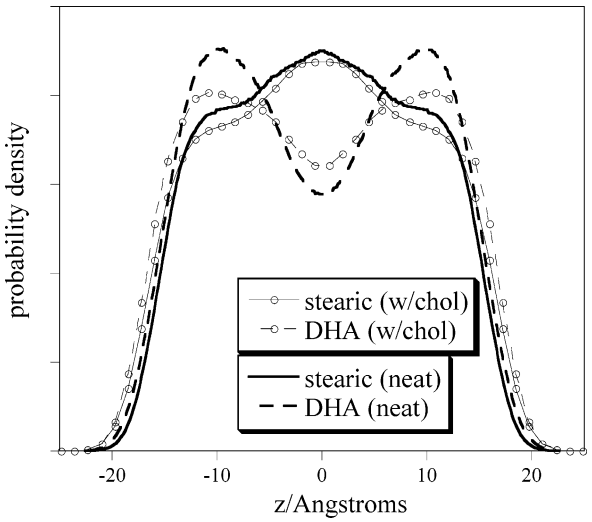

FIGURE 3: Distribution of stearic acid (solid lines) and docosohexaenoic acid (dashed lines) as a function of position along the *z*-coordinate (bilayer normal). The lines with circles give the results for the SDPC/cholesterol system, while the thicker lines give the results of a previously published simulation of neat SDPC (*11*).

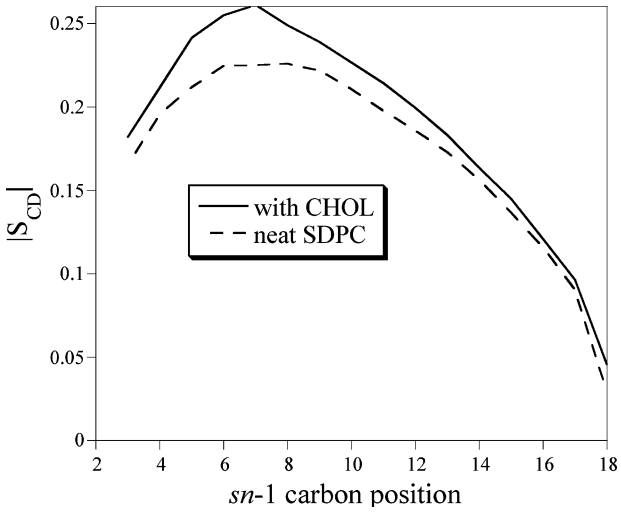

FIGURE 4: Deuterium order parameter, S_{CD}, as a function of position along the saturated *sn*-1 fatty acid chain. The dashed line gives the result of an earlier simulation of neat SDPC, while the solid line shows the modest increase in chain order upon addition of cholesterol.

of the lipid carbonyls is in agreement with additional neutron scattering experiments carried out on a saturated system, dimyristoylphosphatidylcholine (DMPC) (*31*). Thus, it appears that the location of the cholesterol within the membrane is represented realistically based on available experimental data, and that the depth of cholesterol insertion does not depend on the degree of unsaturation, at least at the *sn*-2 position.

The preceding results, both experimental and computational, suggest cholesterol has a strong preference for its transverse position in the membrane. To show how the phospholipid component of the bilayer adjusts to accommodate the sterol, the probability distributions (along the bilayer normal) for the stearoyl and docosohexaenoyl chains are given in Figure 3 for both our simulation and an earlier simulation of neat SDPC (*11*). The striking difference between the distribution of saturated chain density and polyunsaturated chain density has been discussed previously and verified experimentally for the case of neat SDPC (*19*). This simulation shows that the effect of cholesterol on the phospholipid acyl chains is highly nonuniform; the saturated chain shows only a negligible effect (essentially a slight increase in the projected length along the bilayer normal), while the DHA chain undergoes a significant redistribution of its chain segments from the interfacial region to the hydrophobic core of the bilayer. These observations can be understood on the basis of the unique conformational energetics of the DHA chain. Quantum mechanical calculations have shown that the structural motif found in polyunsaturated alkyl chains, namely, double bonds separated by two single bonds, leads to a torsional potential energy surface unlike that of saturated carbon chains. Two very broad energy minima are observed with a large region of torsional space accessible at energies on the order of *kT* (*11*). Thus, the DHA chain can adopt a diverse set of chain conformations with similar (low) energies, while the saturated stearic has a comparatively reduced conformational freedom. As cholesterol is incorporated into the membrane, the highly flexible DHA chain is able to rearrange at little energy cost and vacates sufficient density at the interface to allow space for cholesterol. The mixed chain saturated/polyunsaturated lipid is thus able to adapt to the presence of cholesterol with a much smaller impact on its hydrophobic thickness than a disaturated lipid would (consistent with observations from NMR described in the next paragraph). Experimental measurements of the change in hydrophobic thickness upon addition of cholesterol to disaturated lipids show significant increases in hydrophobic thickness (*28*), and a recent MD simulation of cholesterol in DPPC (at the higher concentration of 40 mol %) showed an 8−9 Å increase upon incorporation of cholesterol (*30*). Our simulation, however, shows a hydrophobic thickness that is increased by less than 2 Å, suggesting a possible role for polyunsaturates is to regulate the hydrophobic thickness of the membrane as the cholesterol content varies.

The effect of cholesterol on phospholipids, saturated at the *sn*-1 position with varying levels of unsaturation on the *sn*-2 chain, has been studied by Huster, Arnold, and Gawrisch (*32*) using NMR techniques. Their principal findings follow. (1) The NMR order parameters of the saturated chain were increased only half as much upon cholesterol addition when paired with the polyunsaturated DHA chain as compared with the monounsaturated oleic acid chain, and (2) cholesterol interacts preferentially with the saturated *sn*-1 chain, promoting lateral organization of the membrane bilayer (*32*). The deuterium NMR order parameter, S_{CD}, measured in their experiments from the quadrupolar splitting, can be directly obtained from the simulation trajectory through the relation

$$S_{CD} = \left\langle \frac{3}{2}\cos^2\theta - \frac{1}{2} \right\rangle \quad (1)$$

where θ is the angle between the C−H bond vector and the bilayer normal and the brackets denote an averaging over time and over all lipids. The order parameters as a function of carbon position are plotted in Figure 4 for both our simulation and the previously reported simulation of neat SDPC. The increase in chain order of ∼10% is quite modest compared to reports from experimental and simulation studies of disaturated PC where increases approaching 100% have

been reported (*30*). Additionally, the effect on the order parameters occurs primarily in the upper half of the acyl chain, consistent with the most likely location of the cholesterol molecule (Figure 2). A direct comparison with experiment is not possible for the SDPC/cholesterol system; however, Huster et al. (*32*) report an order parameter increase of ~15% for the *sn*-1 chain of SDPC in a mixture of phosphatidylcholine, phosphatidylethanolamine, and phosphatidylserine lipids. They note that experiments on lipids differing only in the level of *sn*-2 unsaturation show a 2-fold greater increase in stearoyl order parameters for monounsaturated *sn*-2 chains as opposed to polyunsaturated *sn*-2 chains, a result consistent with the hypothesis that DHA chain flexibility allows a perturbation of the stearoyl chain (Figure 3) much smaller than that which would occur when paired with a saturated or monounsaturated fatty acid.

A more direct experimental probe of differential interactions between cholesterol and saturated/polyunsaturated fatty acids comes from the nuclear Overhauser enhancement spectroscopy (NOESY) cross-relaxation rate measurements of Huster et al. (*32*). They measured the cross-relaxation rate, σ_{IJ}, between the cholesterol C18 methyl resonance and the chain methylene resonances of the stearic acid and DHA. The cross-relaxation rates depend sensitively on the distance between protons and the correlation time for the relaxation of the internuclear vector (*22*). The cross-relaxation rates are determined by the spectral density, $J_{IJ}(\omega)$

$$\sigma_{IJ} = \zeta\left[3J_{IJ}(2\omega_0) - \frac{1}{2}J_{IJ}(0)\right] \qquad (2)$$

where ω_0 is the proton Larmor frequency and $\zeta = (2\pi/5)\gamma^4\hbar^2(\mu_0/4\pi)^2$, where γ is the gyromagnetic ratio. The spectral density is given by the Fourier transform of the sum of autocorrelation functions for the magnetic dipole−dipole interactions between all spins of resonances I and J

$$J_{IJ}(\omega) = \int_{-\infty}^{\infty} C_{IJ}(t)\cos(\omega t)\,dt$$

$$C_{IJ}(t) = \frac{4}{5}\sum_i\sum_j\left\langle \frac{Y_{20}[\vec{r}_{ij}(0)]}{r_{ij}^3(0)}\,\frac{Y_{20}[\vec{r}_{ij}(t)]}{r_{ij}^3(t)}\right\rangle \qquad (3)$$

where $Y_{20} = (5/16\pi)^{1/2}(3\cos^2\theta - 1)$ and θ is the angle between the internuclear vector, $\vec{r}_{ij}$, and the z-axis (normal to the membrane). The $C_{IJ}(t)$ values defined in eq 3 were calculated from the MD simulation and are plotted in Figure 5 for the cholesterol C18 protons with the methylene protons of the saturated and polyunsaturated chains. The correlation function shows that the simulation predicts a rate of magnetization transfer between cholesterol and saturated chain (solid line) methylene groups approximately 2-fold greater than that of transfer in the polyunsaturated chain (dashed line), in excellent agreement with the experimental measurements of Huster et al. (*32*). Furthermore, the simulated correlation functions show equal decay rates; i.e., they differ in magnitude by a near-constant factor of 2. This indicates that the difference in cross-relaxation rates arises due to more frequent close contacts between cholesterol and the saturated fatty acid (as opposed to originating from a difference in the relaxation rate of the internuclear vector). A molecular graphic that nicely captures the intimate contact between cholesterol and the saturated stearoyl chain is

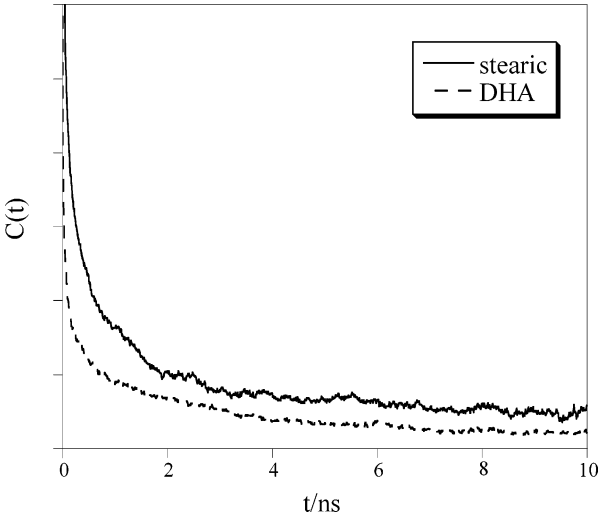

FIGURE 5: Correlation function for the dipolar interaction between methylene protons of the lipid acyl chains and the cholesterol methyl group at C18. The solid and dashed lines give the result for the methylene segments of the saturated *sn*-1 chain and polyunsaturated *sn*-2 chain, respectively.

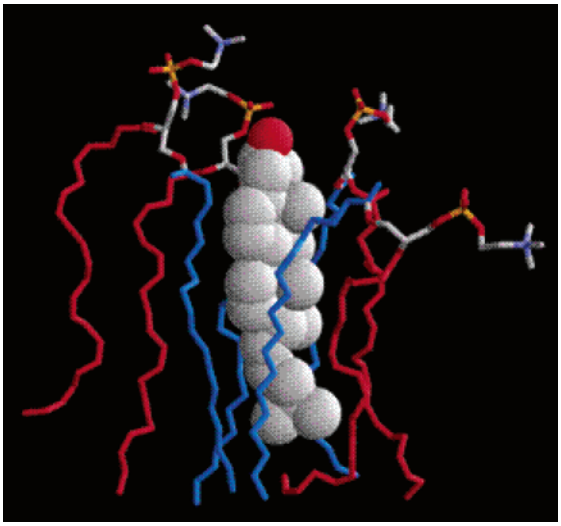

FIGURE 6: Molecular graphic showing the preferential solvation of cholesterol by saturated fatty acids (blue) over polyunsaturated chains (red).

presented in Figure 6. The strength of the cholesterol-saturated chain attraction is more fully appreciated when one considers that the 2-fold increase in the number of close contacts for stearic acid over DHA is accomplished despite the fact that the bulk density of DHA segments is greater than that of stearic acid in the interfacial region where cholesterol resides (Figure 3).

As described in the preceding paragraphs, the simulated membrane exhibited a significant degree of organization due to both the hydrogen bonding ability of cholesterol and the hydrophobic packing interactions of cholesterol's ring system. In this section, we examine the local structure of the cholesterol environment through the construction of probability density (PD) functions. We then analyzed the combined PDs by calculating isosurfaces at selected contour levels to visualize the full spatial distribution. The PD distributions were prepared by registering the full set of coordinates at 10 ps intervals over the last 12 ns of simulation in a consistent frame of reference for each of the 24

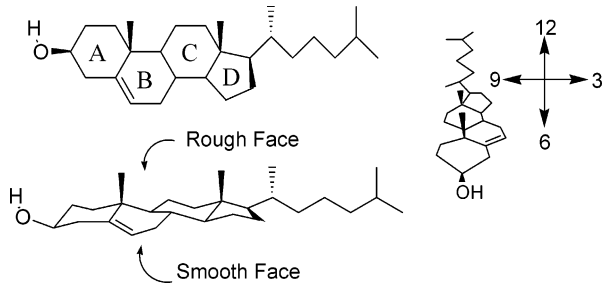

FIGURE 7: Three views of the cholesterol molecule, indicating the system used to describe the probability density isosurfaces in Figures 8−12.

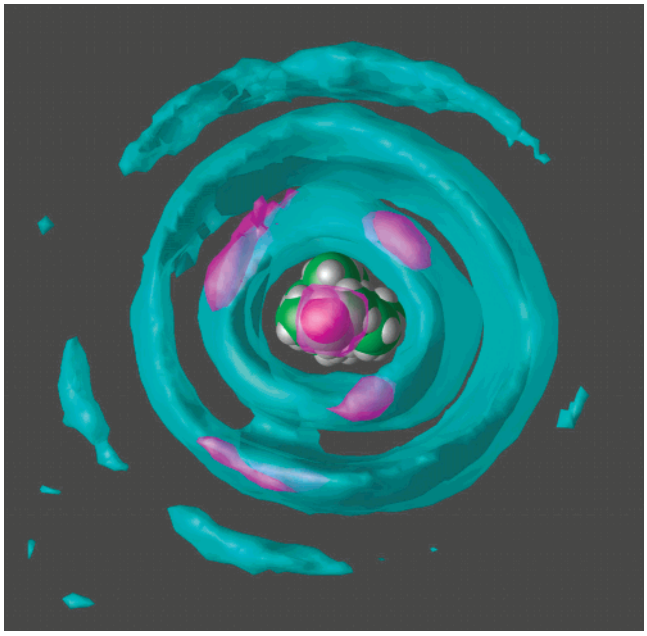

FIGURE 8: Probability density isosurfaces for acyl chains (cyan) and cholesterol molecules (magenta) as a function of the distance from, and orientation with respect to, the cholesterol molecule (space filling representation), showing several layers of lipids solvating the sterol.

cholesterols present in the simulation. The frame of reference for each cholesterol was defined by orienting the C18 methyl bond vector along the *x*-axis and the C10 carbon in the *x*−*z* plane (right-handed coordinate system). Registration of the coordinates in a frame common to each cholesterol allows the environments to be combined into one PD distribution. The distributions were normalized to allow comparisons at the same isosurface contour value for different distributions. To compare isosurfaces, we rendered red and blue isosurfaces slightly transparent, so that regions in common appear purple due to color mixing.

The structure of lipid solvent shells around cholesterol conveys a great deal about their interaction during the simulation. Figure 8 shows a high-value isosurface contour of the lipid environment (combined acyl chains) around cholesterol. A reference cholesterol is shown as space-filling spheres (in a representative conformation) to provide context. The rippled cyan surface in Figure 8 encloses the regions of high likelihood for lipid density, and directly indicates solvation shells. As the contour level is reduced (data not shown), several shells continue to emerge over the entire length of the simulation cell with clear resolution, indicating that cholesterol induces order on a length scale greater than

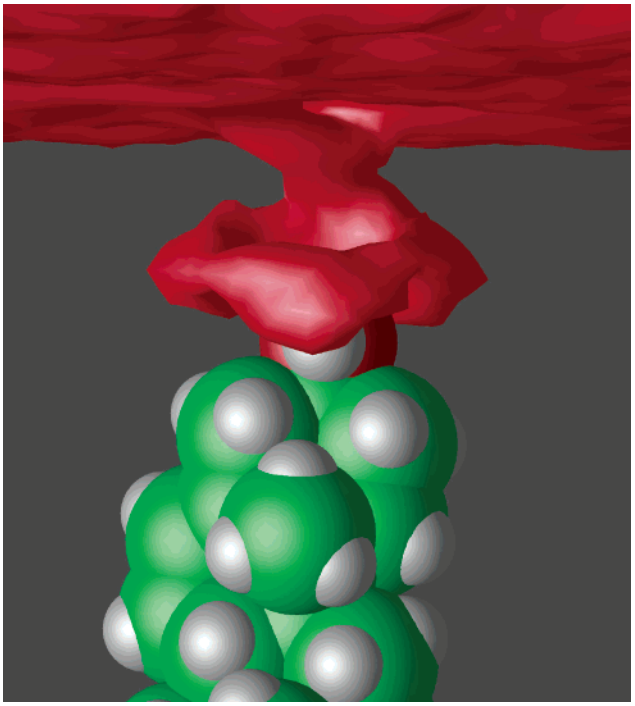

FIGURE 9: Probability density isosurface for water (red) as a function of the distance and orientation around the cholesterol molecule, showing the frequent interactions between water molecules and the cholesterol hydroxyl group.

at least a few nanometers. The magenta regions in Figure 8 are the highest-probability regions for neighboring cholesterol C−O density. As a descriptive aid, consider the numbers on the face of a clock superimposed on the top view of cholesterol, with the two methyl groups indicating the 12 o'clock position (see Figure 7). The 3-fold symmetry of the three regions at 1−2, 5, and 10 o'clock positions on the first solvation shell shows the three most common orientations and/or distances for cholesterol−cholesterol coordination. The radial distribution for cholesterol O−O distances peaks at roughly 5 Å for the first solvation shell, which is too far for direct hydrogen bonding to be significant. The cholesterol−cholesterol interaction is therefore primarily hydrophobic. The two methyl groups on the rough face, defining the 12 o'clock position, form a ridge along the ring system giving cholesterol a wedge shape. The three wedge faces are fairly perpendicular to the O−O directions, which is consistent with face-to-face interactions for cholesterol dimers.

Figure 9 shows the front (12 o'clock) view of the water PD. While the cholesterol−water hydrogen bonding appears to have little angular anisotropy, there does appear to be a slightly preferred orientation of water approach at the 12 o'clock position. This can be seen as a region extending from the bulk through the 6 o'clock position. Note that overall, the cholesterol appears to be quite dry; i.e., the surface area that is hydrated is small compared to the molecular cross-sectional area. Water penetration between cholesterols was not a common event in this simulation (see bilayer profile distributions above).

Figure 10 shows the interaction of cholesterol with the phosphate oxygen (gold) and choline methyl (gray) groups viewed from the 11 o'clock and top, respectively. A lobe of high probability from the phosphate occupies the same 12 o'clock position as water (see Figure 9), suggesting the

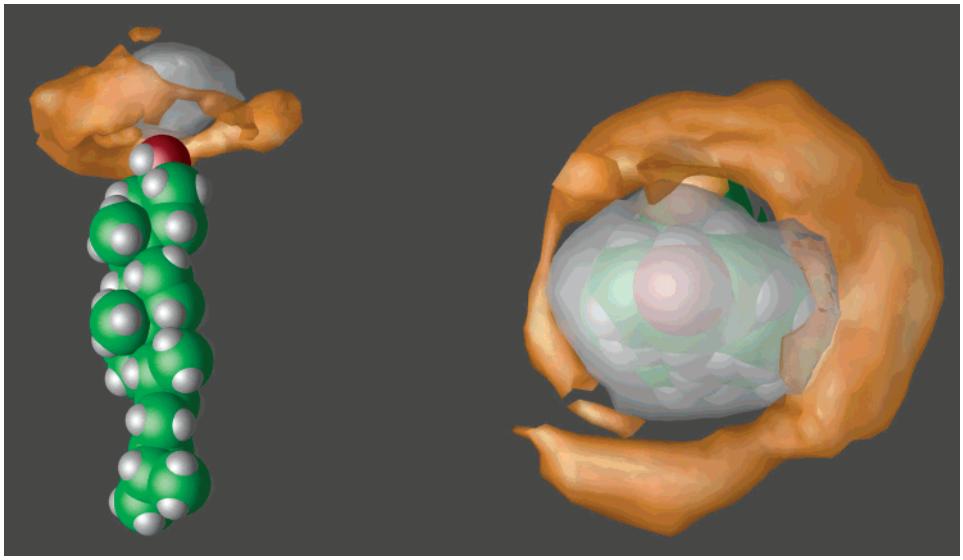

FIGURE 10: Probability density isosurface for phosphate (gray) and choline (gold) atoms as a function of the distance and orientation around the cholesterol molecule, showing the hydrogen bonding between cholesterol hydroxyl and phosphate oxygens and the covering of the sterol by the choline.

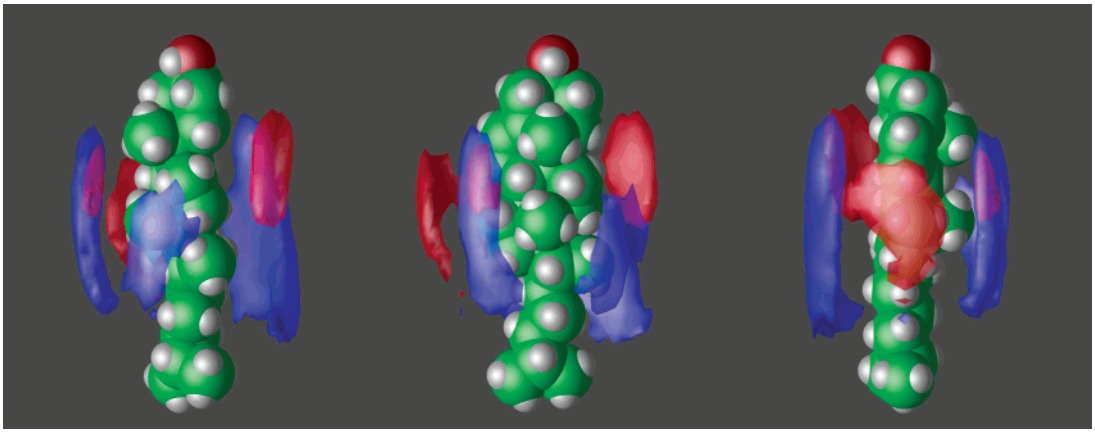

FIGURE 11: Probability density isosurface for stearic (blue) and DHA (red) acyl chains as a function of the distance and orientation around the cholesterol molecule, showing distinct regions where the individual chains solvate the sterol. The three orientations shown are as described in the text.

cholesterol molecule has a significant orientational preference in its hydrogen bonding with both lipid and water. The relatively larger distances of the remaining regions of phosphate density imply that at best weak hydrogen bonds may exist in orientations other than the 12 o'clock position. The top view shows that the cholesterol surface is covered by the hydrophilic phosphocholine of the lipids. Thus, in these simulations, the choline group appears to interact in a nonspecific fashion, in contrast to the strong hydrogen bonding between choline and the cholesterol hydroxyl observed in the DPPC/cholesterol bilayer simulation of Berkowitz and co-workers (*30*), though the choline and phosphate distributions near cholesterol might imply a phosphate−choline−cholesterol complex is common in these simulations.

Figure 11 shows 10, 12, and 3 o'clock views of the high-probability regions for DHA (red) and stearic (blue) acyl chain segments. Figure 12 shows a lower-contour view of the same data and color scheme from a different orientation. There is a preference for the stearic acid along the 6 o'clock or smooth face [consistent with experimental observations of Endress et al. (*33*)] and additionally along the 2 o'clock face. The DHA chain appears to occupy the remaining regions with little close contact (cleanly separable at high contour levels). The lower-contour view of Figure 12 shows more overlap, but the orientational preference is even more pronounced.

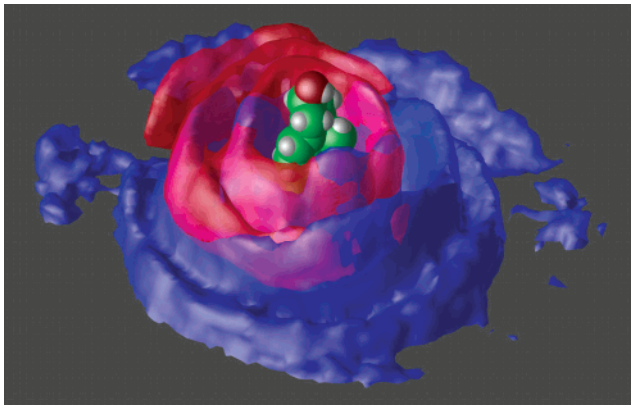

FIGURE 12: Probability density isosurface for stearic (blue) and DHA (red) acyl chains as a function of the distance and orientation around the cholesterol molecule, showing the preference for the sterol to be solvated by the saturated acyl chain. Regions that appear purple are overlapping blue and red surfaces.

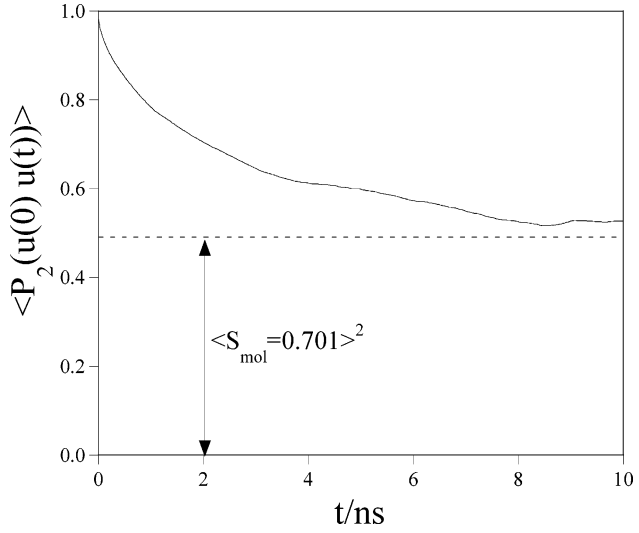

FIGURE 13: Second rank reorientational correlation function for the principal (long) axis of the cholesterol molecule. The plateau value, calculated from the square of the molecular order parameter, indicates the point to which the correlation function would decay.

We have studied the dynamics of the cholesterol molecule and the effect of cholesterol on lipid dynamics through the calculation of various time correlation functions from the simulation trajectory. Turning first to the cholesterol molecule, we examine its rotational dynamics by following the principal axis of its moment of inertia tensor, i.e., the long axis of the molecule. Figure 13 gives the second rank reorientational correlation function $\{C(t) = \langle P_2[\vec{\mu}(0)\cdot\vec{\mu}(t)]\rangle\}$ for the cholesterol principal axis, demonstrating a multinanosecond correlation time for cholesterol reorientation. The ordering effect of the membrane prevents full relaxation of the principal axis vector leading to a plateau value equal to the square of an order parameter that we have denoted S_{mol} (this order parameter is defined in the same manner as the CD bond order parameters discussed earlier; however, in this case, the principal axis vector is used rather than the CD bond vector). The observation that the correlation function in Figure 13 nearly reaches the plateau value demonstrates that the cholesterol molecule is axially averaged on the time scale of this simulation. In addition to S_{mol}, the cholesterol orientation can also be described in more detail by the distribution of tilt angles observed in the simulation (Figure 14A) and its corresponding potential of mean force (Figure 14B). This figure shows that while the membrane structure has a strong ordering effect on the cholesterol, substantial tilt angles are possible with an only moderate energy cost and an average tilt angle of 25° is observed in the simulation. The tilt angle of cholesterol in an SDPC bilayer has been investigated by Brzustowicz et al. by measurement of the deuterium order parameter of cholesterol labeled at the 3α position (*34*). In a 50 mol % cholesterol system at 20 °C, they observe $|S_{CD}| = 0.35$, and from this estimate, a most probable tilt angle of 16° from a model that assumes the order parameter can be written as the product of the molecular order parameter and a geometrical factor arising from the geometry of the C−D bond. The values obtained from our simulation ($|S_{CD}| = 0.26$ and a tilt angle of 25°) are consistent with the greater disorder expected at this decreased cholesterol concentration (25 mol %) and increased temperature (37 °C).

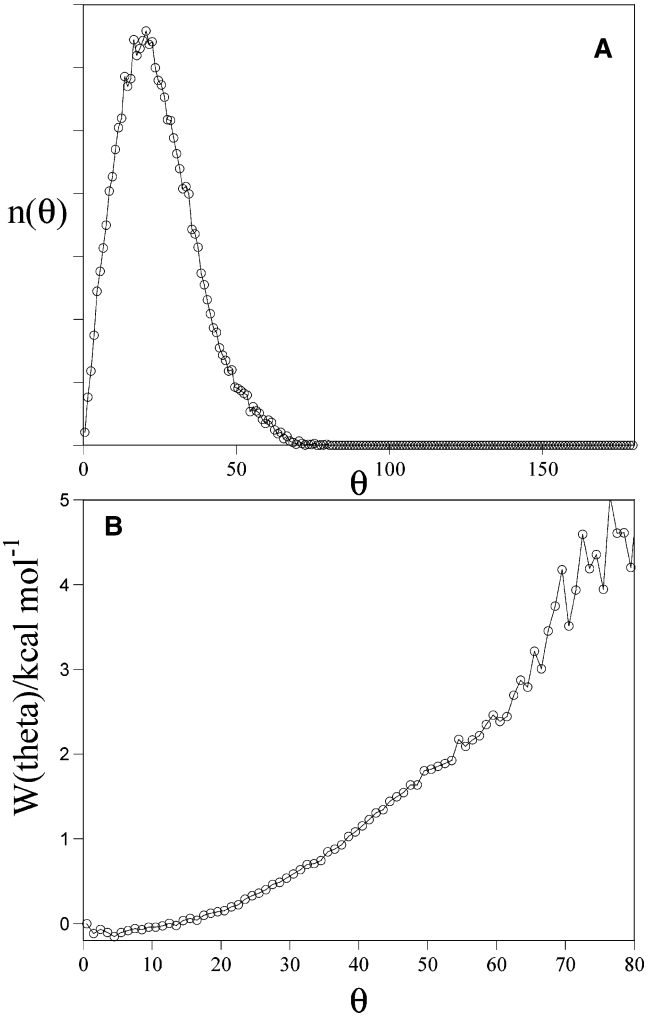

FIGURE 14: (A) Histogram of orientations of the principal axis of the cholesterol molecule with respect to the bilayer normal, showing an average orientation of 25°. (B) Potential of mean force for cholesterol orientation with respect to the bilayer normal.

The translational motion of the cholesterol molecule can be separated into components parallel and perpendicular to the membrane. The displacements perpendicular to the membrane have magnitudes of several angstroms and contribute significantly to the width of the distribution function for cholesterol in Figure 2. Calculation of the autocorrelation function for these transverse fluctuations shows a relaxation time of just <2 ns (data not shown). Cholesterol and lipid translational motion within the plane of the membrane is quantified through the mean square displacement correlation function after removal of the center-of-mass drift of each leaflet from its constituent lipid and cholesterol molecules. The diffusion constant at time τ in two dimensions is given by

$$D(\tau) = \frac{1}{4}\frac{\langle|\vec{r}(t_0+\tau) - \vec{r}(t_0)|^2\rangle}{\tau} \qquad (4)$$

where the brackets represent an ensemble average over all lipids and all initial times, t_0. Although the calculation of D as a mean is straightforward, its standard error is more elusive because of the coherence in the trajectory. To treat this coherence formally while still performing an automated procedure that samples uniformly from all trajectories and

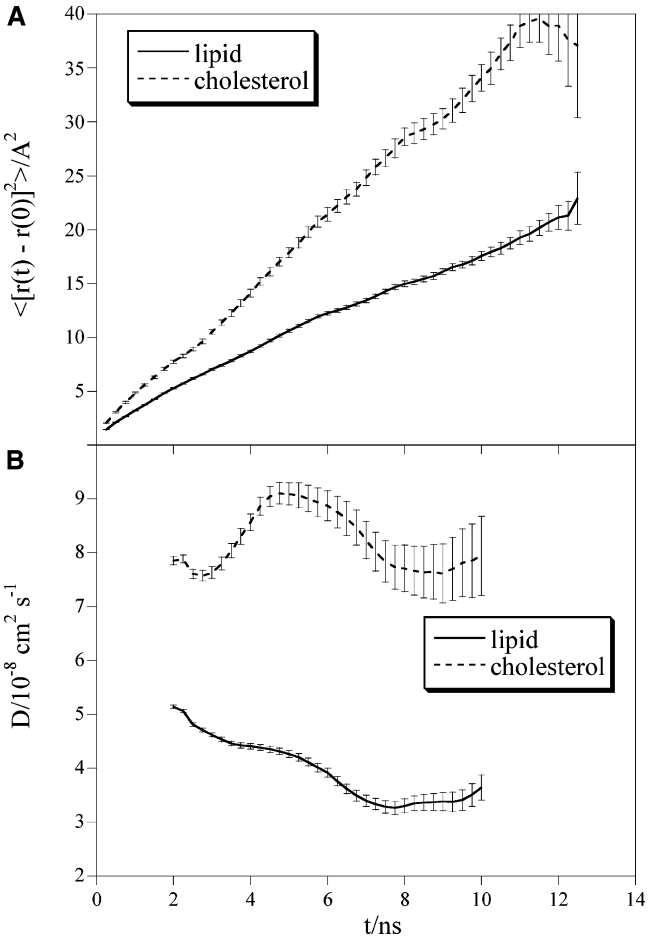

FIGURE 15: (A) Mean square displacement as a function of time calculated from the lipid (solid line) and cholesterol (dashed line) centers of mass. (B) Diffusion constant, calculated as a function of lag time, *t*, for the lipid (solid line) and cholesterol (dashed line) molecules.

all times, we made novel use of the bootstrap statistical technique (*35*) to construct an ensemble of ensembles, and used the standard deviation of the resulting means as an estimate of the standard error in the simulation. To construct a single bootstrap ensemble for a given time spacing, τ, we first assumed an approximate translational coherence time of 1 ns, which provided an estimate of the number of independent samples in each trajectory. For these diffusion calculations, we used the final 12 ns of the simulation, so the approximate number of independent samples in each trajectory is 12. We then randomly chose from the ensemble $12N$ pairs of coordinates separated by τ, each individual pair chosen from the same trajectory, but at an arbitrary starting time in that trajectory; N is the number of constituent molecules: 24 for cholesterol and 72 for lipids. Each individual bootstrap ensemble has its own mean, and the standard deviation of the mean of many such ensembles (we chose 200 for this study) reflects the standard error of the fundamental observable. Figure 15 (top panel) shows the resulting plot of r^2 versus τ with the means and standard error obtained by the bootstrap technique, for both cholesterol and lipid. To estimate D in the limit of large τ, we then calculated the slope of the curve at each point based on the local range of ± 2 ns, and weighted by the standard error at each point, to provide a corresponding mean and standard error in D, shown in Figure 15 (bottom panel). It is evident from the plots that the extent of diffusion of cholesterol is significantly greater than that of the lipid [$(3.6 \pm 0.2) \times 10^{-8}$ cm/s^2 for the lipid and $(7.9 \pm 0.7) \times 10^{-8}$ cm/s^2 for cholesterol, based on the slope of r^2 when $\tau = 10$ ns]. These values are in line with experimental measurements of $5-30 \times 10^{-8}$ cm/s^2 (*33*). The magnitude of the uncertainties increases when the calculation is repeated assuming longer coherence times (data not shown); however, the results are qualitatively similar with a statistically significant difference between sterol and phospholipids observed even when the coherence time is increased by an order of magnitude.

The effect of cholesterol on lipid dynamics provides further evidence of cholesterol's affinity for saturated chains over polyunsaturated fatty acids. The reorientation correlation functions for representative CH vectors on the fatty acid chains have been calculated, and compared with earlier simulation results for a neat SDPC bilayer. The effect of cholesterol on the saturated stearic acid chain is to slow its motions (data not shown), in agreement with earlier simulations of disaturated PC (*18*); however, cholesterol's effect on the DHA chain is significantly smaller in magnitude. While the impact of the cholesterol is greater on the saturated chain, the effect is much smaller than that observed with disaturated lipids, consistent with the idea that DHA acts to disorder the membrane to such an extent that even in the presence of 25 mol % cholesterol a very fluid bilayer is maintained.

DISCUSSION

We have developed empirical force field parameters for cholesterol, a molecule of extreme biological importance, and tested these against NMR observables calculated from a long, stable molecular dynamics computer simulation. Our primary conclusions are that (1) cholesterol has a much higher affinity for saturated fatty acids that arises from differences in packing of the hydrophobic core, specifically the smooth faces of the sterol ring system, and (2) DHA acts to reduce the impact that cholesterol has on the phospholipid bilayer, allowing incorporation of sterol into the membrane while minimizing changes in hydrophobic thickness and membrane viscosity. By comparing these results with simulation results for neat SDPC, we see that DHA chain segments move toward the bilayer center when cholesterol is added, consistent with a low affinity for cholesterol. Our analysis of the correlation function underlying the NOESY cross-relaxation rates confirms the interpretation of these experiments, namely, that cholesterol's close contacts with acyl chains are predominantly with saturated methylene groups. An interesting question is the extent to which these observations depend on the number of double bonds versus the placement of the double bonds. The hydrogen bonding requirements of the sterol hydroxyl group seem to require a location in the upper acyl chain region for the rigid ring system; thus, it is possible that a chain polyunsaturated only in its lower end (such as α-linolenic) may be able to interact with cholesterol in a manner more similar to that of a saturated chain. Differences have been observed, however, in the structure and dynamics of lipid bilayer membranes upon removal of one double bond (*19*). Thus, a unique relationship between cholesterol and DHA cannot be ruled out.

Cholesterol's selectivity for the saturated and polyunsaturated chains, along with its orientational dependence, appears to have important consequences in the ordering and structure of the bilayer. Specifically, cholesterol's affinity for saturated chains increases the likelihood of saturated chains being found at certain regions in the inner solvation shell of cholesterol. The smooth face is the most likely, but a region between the B ring and the ring methyl groups is another. The preference for saturation of the smooth face consequently increases the likelihood of polyunsaturation in the second solvation shell on the smooth face. The accumulation of polyunsaturation on the smooth face of cholesterol is balanced by an increased level of saturation on the rough face. These results therefore suggest a possible mechanism via which cholesterol affects long-range order in terms of local and relatively simple interactions. The increased affinity for saturated chains creates a compositional bias that propagates over several solvation shells. The picture that emerges from these simulations is in many ways similar to the model proposed by Mitchell and Litman (*36*), who proposed that lateral microdomains could form solely on the basis of the relative strength of cholesterol−acyl chain interactions. As emphasized by Mitchell and Litman, these microdomains are not static but rather are constantly exchanging members, a view supported by our simulations in which radial and orientational structure is observed around the sterols while at the same time the bilayer maintains a high degree of disorder where lipid species rapidly diffuse in the plane of the membrane.

It is interesting to question whether cholesterol has a similar effect on the more studied symmetrically disubstituted membranes (such as DPPC), or whether the differential affinity for chain saturation enables ordering or structural properties that are less accessible with mixtures of symmetrical disubstituted lipids. The differences observed between this simulation of SDPC and the numerous reports in the literature of DPPC simulations indicate qualitatively different behavior between these two systems. One possible reason the SDPC and similar asymmetrically substituted lipids may be qualitatively different from a symmetrically disubstituted lipid with the same composition (e.g., 1:1 DSPC/DDPC) is that with a symmetrically disubstituted lipid, cholesterol may be effectively screened by a local concentration of saturated chains, leaving the polyunsaturated lipids free to diffuse with minimal cholesterol interaction. An asymmetrically substituted environment prevents complete screening of cholesterol and forces even composition at the length scale of individual lipids. The dual character of asymmetrically disubstituted lipids, when organized by an agent with a preferential affinity for saturation, can propagate a local preference to a larger length scale. This process may be a more general mechanism for inducing order in membranes of other compositions as well.

ACKNOWLEDGMENT

We acknowledge the support of the Blue Matter Team (Blake G. Fitch, Robert S. Germain, Alex Rayshubskiy, T. J. Chris Ward, Yuri Zhestkov, Maria Eleftheriou, Jed W. Pitera, and William C. Swope).

SUPPORTING INFORMATION AVAILABLE

Tables of data for cholesterol and related compounds. This material is available free of charge via the Internet at http://pubs.acs.org.

REFERENCES

1. Bergelson, L. O., Gawrisch, K., Ferretti, J. A., and Blumenthal, R. (1995) Domain organization in biological membranes, *Mol. Membr. Biol. 12*, 1−162.
2. Simons, K., and Ikonen, E. (1997) Functional rafts in cell membranes, *Nature 387*, 569−572.
3. Brzustowicz, M. R., Cherezov, V., Caffrey, M., Stillwell, W., and Wassall, S. R. (2002) Molecular organization of cholesterol in polyunsaturated membranes: microdomain formation, *Biophys. J. 82*, 285−298.
4. Litman, B. J., and Mitchell, D. C. (1996) A role for phospholipids polyunsaturation in modulating membrane protein function, *Lipids 31*, S193−S197.
5. Shaikh, S. R., Cherezov, V., Caffrey, M., Stillwell, W., and Wassall, S. R. (2003) Monounsaturated PE does not phase separate from the lipid raft molecules sphingomyelin and cholesterol: role for polyunsaturation? *Biochemistry 42*, 12028−12037.
6. Menkes, J. H., Alter, M., Steigleder, G. K., Weakley, D. R., and Sung, J. H. (1962) A sex-linked recessive disorder with retardation of growth, peculiar hair and focal cerebral and cerebellar degeneration, *Pediatrics 29*, 764−779.
7. Birch, E. E., Birch, D. G., Hoffman, D. R., and Uauy, R. (1992) Dietary essential fatty acid supply and visual acuity development, *Invest. Ophthalmol. Visual Sci. 33*, 3242−3253.
8. Kremer, J. M., Lawrence, D. A., Jubiz, W., DiGiaccomo, R., Rynes, R., Bartholomew, L. E., and Sherman, M. (1990) Dietary fish oil and olive oil supplementation in patients with rheumatoid arthritis, *Arthritis Rheum. 33*, 810−820.
9. Freedman, S. D., Katz, M. H., Parker, E. M., Laposata, M., Urman, M. Y., and Alvarez, J. G. (1999) A membrane lipid imbalance plays a role in the phenotypic expression of cystic fibrosis in cftr(−/−) mice, *Proc. Natl. Acad. Sci. U.S.A. 96*, 13995−14000.
10. Stillwell, W., and Wassall, S. R. (2003) Docosahexaenoic acid: membrane properties of a unique fatty acid, *Chem. Phys. Lipids 126*, 1−27.
11. Feller, S. E., Gawrisch, K., and MacKerell, A. D. (2002) Polyunsaturated fatty acids in lipid bilayers: intrinsic and environmental contributions to their unique physical properties, *J. Am. Chem. Soc. 124*, 318−326.
12. Feller, S. E., Gawrisch, K., and Woolf, T. B. (2003) Rhodopsin exhibits a preference for salvation by polyunsaturated docosohexaenoic acid, *J. Am. Chem. Soc. 125*, 4434−4435.
13. Schlenkrich, M., Brickmann, J., MacKerell, A. D., Jr., and Karplus, M. (1996) Empirical potential energy function for phospholipids: criteria for parameter optimization and applications, in *Biological Membranes: A Molecular Perspective from Computation and Experiment* (Merz, K. M., and Roux, B., Eds.) pp 31−81, Birkhäuser, Boston.
14. Feller, S. E., and MacKerell, A. D., Jr. (2000) An improved empirical potential energy function for molecular simulations of phospholipids, *J. Phys. Chem. B 104*, 7510−7515.
15. Feller, S. E., Yin, D. X., Pastor, R. W., and MacKerell, A. D. (1997) Molecular dynamics simulation of unsaturated lipid bilayers at low hydration: parametrization and comparison with diffraction studies, *Biophys. J. 73*, 2269−2279.
16. Brooks, B. R., Bruccoleri, R. E., Olafson, B. D., States, D. J., Swaminathan, S., and Karplus, M. (1983) CHARMM: A program for macromolecular energy, minimization, and dynamics calculations, *J. Comput. Chem. 4*, 187−217.
17. MacKerell, A. D., Jr., Brooks, B., Brooks, C. L., III, Nilsson, L., Roux, B., Won, Y., and Karplus, M. C. (1998) in *Encyclopedia of Computational Chemistry* (Schleyer, P., Ed.) pp 271−277, John Wiley & Sons, Chichester, U.K.
18. Tu, K., Klein, M. L., and Tobias, D. J. (1998) Constant-pressure molecular dynamics investigation of cholesterol effects in a dipalmitoylphosphatidylcholine bilayer, *Biophys. J. 75*, 2147−2156.
19. Eldho, N. V., Feller, S. E., Tristram-Nagle, S., Polozov, I. V., and Gawrisch, K. (2003) Polyunsaturated docosohexaenoic vs docosopentaenoic acid: differences in lipid matrix properties from the loss of one double bond, *J. Am. Chem. Soc. 125*, 6409−6421.

20. Feller, S. E., Venable, R. M., and Pastor, R. W. (1997) Computer simulation of a DPPC phospholipid bilayer: structural changes as a function of molecular surface area, *Langmuir 13*, 6555−6561.
21. Fitch, B. G., Germain, R. S., Mendell, M., Pitera, J., Pitman, M., Rayshubskiy, A., Sham, Y., Suits, F., Swope, W., Ward, T. J. C., Zhestkov, Y., and Zhou, R. (2003) Blue Matter, an application framework for molecular simulation on Blue Gene, *J. Para. Distrib. Comp. 63*, 759−773.
22. Feller, S. E., Huster, D., and Gawrisch, K. (1999) Interpretation of NOESY cross-relaxation rates from molecular dynamics simulation of a lipid bilayer, *J. Am. Chem. Soc. 121*, 8963−8964.
23. Moore, P. B., Lopez, C. F., and Klein, M. L. (2001) Dynamical properties of a hydrated lipid bilayer from a multinanosecond molecular dynamics simulation, *Biophys. J. 81*, 2484.
24. Kuczera, K., Wiorkiewicz, J. K., and Karplus, M. (1993) *MOLVIB: Program for the Analysis of Molecular Vibrations*, *CHARMM*, Harvard University, Cambridge, MA.
25. Pulay, P., Fogarasi, G., Pang, F., and Boggs, J. E. (1979) Systematic ab initio gradient calculation of molecular geometries, force constants, and dipole moment derivatives, *J. Am. Chem. Soc. 101*, 2550−25604.
26. Frisch, M. J., Trucks, G. W., Schlegel, H. B., Scuseria, G. E., Robb, M. A., Cheeseman, J. R., Zakrzewski, V. G., Montgomery, J. A., Jr., Stratmann, R. E., Burant, J. C., Dapprich, S., Millam, J. M., Daniels, A. D., Kudin, K. N., Strain, M. C., Farkas, O., Tomasi, J., Barone, V., Cossi, M., Cammi, R., Mennucci, B., Pomelli, C., Adamo, C., Clifford, S., Ochterski, J., Petersson, G. A., Ayala, P. Y., Cui, Q., Morokuma, K., Malick, D. K., Rabuck, A. D., Raghavachari, K., Foresman, J. B., Cioslowski, J., Ortiz, J. V., Stefanov, B. B., Liu, G., Liashenko, A., Piskorz, P., Komaromi, I., Gomperts, R., Martin, R. L., Fox, D. J., Keith, T., Al-Laham, M. A., Peng, C. Y., Nanayakkara, A., Gonzalez, C., Challacombe, M., Gill, P. M. W., Johnson, B. G., Chen, W., Wong, M. W., Andres, J. L., Head-Gordon, M., Replogle, E. S., and Pople, J. A. (1998) *Gaussian 98*, Gaussian, Inc., Pittsburgh, PA.
27. Allen, F. H., Bellard, S., Brice, M. D., Cartwright, B. A., Doubleday, A., Higgs, H., Hummelink, T., Hummelink-Peters, B. G., Kennard, O., Motherwell, W. D. S., Rodgers, J. R., and Watson, D. G. (1979) The Cambridge crystallographic data centre: Computer-based search, retrieval, analysis and display of information, *Acta Crystallogr. B35*, 2331−2339.
28. MacKerell, A. D., Jr., Bashford, D., Bellott, M., Dunbrack, R. L., Jr., Evanseck, J., Field, M. J., Fischer, S., Gao, J., Guo, H., Ha, S., Joseph, D., Kuchnir, L., Kuczera, K., Lau, F. T. K., Mattos, C., Michnick, S., Ngo, T., Nguyen, D. T., Prodhom, B., Reiher, I., Roux, W. E. B., Schlenkrich, M., Smith, J., Stote, R., Straub, J., Watanabe, M., Wiorkiewicz-Kuczera, J., Yin, D., and Karplus, M. (1998) All-atom empirical potential for molecular modeling and dynamics studies of proteins, *J. Phys. Chem. B 102*, 3586−3616.
29. MacKerell, A. D., Jr. (2001) Atomistic Models and Force Fields, in *Computational Biochemistry and Biophysics* (Becker, O. M., MacKerell, A. D., Jr., Roux, B., and Watanabe, M., Eds.) pp 7−38, Marcel Dekker, New York.
30. Pandit, S. A., Bostick, D., and Berkowitz, M. L. (2004) Complexation of phosphatidylcholine lipids with cholesterol, *Biophys. J. 86*, 1345−1356.
31. Leonard, A., Escrive, C., Laguerre, M., Pebay-Peyroula, E., Neri, W., Pott, T., Katsaras, J., and Dufourc, E. J. (2001) Location of cholesterol in DMPC membranes: A comparative study by neutron diffraction and molecular mechanics simulation, *Langmuir 17*, 2019−2030.
32. Huster, D., Arnold, K., and Gawrisch, K. (1998) Influence of docosahexaenoic acid and cholesterol on lateral lipid organization in phospholipid mixtures, *Biochemistry 37*, 17299−17308.
33. Endress, E., Heller, H., Casalta, H., Brown, M. F., and Bayerl, T. M. (2002) Anisotropic motion and molecular dynamics of cholesterol, lanosterol, and ergosterol in lecithin bilayers studied by quasi-elastic neutron scattering, *Biochemistry 41*, 13078.
34. Brzustowicz, M. R., Stillwell, W., and Wassall, S. R. (1999) Molecular organization of cholesterol in polyunsaturated phospholipid membranes: A solid state ^{2}H NMR investigation, *FEBS Lett. 451*, 197−202.
35. Efron, B., and Tibshirani, R. J. (1993) *An Introduction to the Bootstrap*, Chapman & Hall/CRC, New York.
36. Mitchell, D. C., and Litman, B. J. (1998) Effect of cholesterol on molecular order and dynamics in highly polyunsaturated phospholipid bilayers, *Biophys. J. 75*, 896−908.

BI048231W